

Paper No.
16656



Effect of Flow on the Corrosion Behavior of Pipeline Steels Under Supercritical CO₂ Environments with Impurities

Martin Colahan, Yoon-Seok Choi, Srdjan Nestic
Institute for Corrosion and Multiphase Technology, Ohio University
342 W State Street
Athens, Ohio, 45701
USA

ABSTRACT

Corrosion is a major concern in transmission pipelines that transport captured CO₂. While dry CO₂ is noncorrosive, significant corrosion has been reported in dense phase CO₂ with trace amounts of water and impurities such as O₂, H₂S, SO_x, and NO_x. The aim of this work is to improve our understanding of the physicochemical aspects on the corrosion of carbon steels in the high-pressure environments associated with CO₂ transmissions pipelines. The effect of flow on the corrosion of X65 carbon steel was investigated in a series of autoclave tests with different combinations of impurity concentrations in supercritical CO₂ condition (8 MPa and 35°C). The corrosion rate of samples was determined by weight loss measurements. The surface morphology and the composition of the corrosion product layers were analyzed by using surface analytical techniques (SEM and EDS). Localized corrosion was measured via surface profilometry after corrosion products were removed. Results showed that no corrosion was observed in the supercritical CO₂ with 650 ppm of water, 50 ppm SO₂, and 100 ppm NO, but corrosion occurred when SO₂ concentration was increased to 4500 ppm and 40,000 ppm of O₂ was added to the system. The presence of flow significantly accelerated the corrosion of carbon steel. Furthermore, localized corrosion was observed in the presence of both O₂ and flow.

Key words: Supercritical Carbon Dioxide, Corrosion, Impurities, Carbon Capture and Storage

INTRODUCTION

It is well known that dry CO₂ does not corrode carbon steels, and negligible corrosion occurred at water-unsaturated conditions (below solubility level) in dense phase CO₂ (liquid and supercritical).¹⁻⁵ However, it has been reported that noticeable, and potentially severe, corrosion occurs at water-unsaturated conditions in dense phase CO₂ with the presence of impurities, such as O₂, H₂S, SO₂, NO₂, etc. due to synergisms between chemical species.⁶⁻¹⁴

Hua, *et al.*,⁸ reported that general corrosion rates ranged from 0 to 0.012 mm/y with water contents varying from 300 ppm to 2800 ppm in the supercritical CO₂ with 1000 ppm O₂. They also found that the general corrosion rates of X65 steel increased from 0.01 mm/y to 0.06 mm/y with water concentration increasing from 300 ppm to 1770 ppm with 100 ppm SO₂ and 20 ppm O₂ at 35°C and 80 bar.⁹ Xu, *et*

al.,¹⁰ reported that the general corrosion rates of X70 steel varied from 0.03 mm/y to 1.78 mm/y at relative humidities ranging from 45% to 100% at 10 MPa CO₂ and 50°C with 2% SO₂ and 1% O₂. Dugstad, *et al.*,¹¹ investigated the corrosion behavior of carbon steel exposed to liquid CO₂ flow for 10 days at 10 MPa and 25°C. The results showed that there was no corrosion in the liquid CO₂ flow with 500 ppm_w H₂O, while adding 500 ppm_w SO₂ induced corrosion at a rate of 0.02 mm/year, and adding 500 ppm_w NO₂ caused severe corrosion with rates reaching 1.6 mm/year. Choi, *et al.*,¹¹ investigated the effect of H₂S on the corrosion behavior of pipeline steels in high pressure CO₂ systems. It was found that the general corrosion rates of the carbon steel and 1Cr steel tested were below 0.01 mm/year with the presence of 100 ppm H₂O and 200 ppm H₂S in the liquid (25°C, 12 MPa) and supercritical (80°C, 12 MPa) CO₂ phases.

Considering that the application of above mentioned studies is the internal corrosion of pipeline related to carbon capture and storage (CCS), enhanced oil recovery (EOR), and deep water oil and gas production, an attempt to evaluate the effect of flow on the corrosion behavior must also be made. Liu *et al.*,¹⁵ investigated the effect of flow rate on steel corrosion in supercritical CO₂ with different water concentrations. The results showed that a higher flow rate significantly enhanced the corrosion rate of carbon steel which is related to a mechanism of water droplet entrainment. However, they investigated only the effect of water without considering other impurities. Sui *et al.*,¹⁶ reported that the wall shear stress formed in the water-saturated supercritical CO₂ system was not enough to damage the formed corrosion product film but affected the morphology of the corrosion product film. The study was conducted in the water-saturated supercritical CO₂ with 1000 ppm H₂S.

There are very limited data on the corrosion behavior in flowing supercritical CO₂ conditions with different impurities. Thus, the objective of the present study was to identify and quantify the effect of flow on the integrity of carbon steel in supercritical CO₂ with different impurities (H₂O, SO₂, O₂ and NO).

EXPERIMENTAL PROCEDURE

The test specimens were machined from UNS K03014 low carbon steel with a size of 12 x 12 x 2.5 mm for the stagnant tests and 25.4 x 12.5 x 3.1 mm for the flowing tests. The specimens were ground with 600 grit silicon carbide paper, cleaned with alcohol in an ultrasonic bath, dried, and weighed using a balance with a precision of 0.1 mg. The solution used in this work corresponded to 650 ppm of DI water in CO₂ phase at the testing pressure and temperature.¹⁷

Experiments were performed in a 7.5L Hastelloy autoclave where the specimens were attached to holders hung from the lid. Pictures of the autoclave corrosion test system used in this study are presented in Figure 1. After the lid was attached, the autoclave was purged by multiple cycles of pressurization with CO₂ and then depressurization. The required volume of N₂-purged deionized water was then added just prior to pressurization with impurities and CO₂. The impurities were added from technical grade (ultra-high purity) sulfur dioxide (SO₂), nitric oxide (NO), and oxygen (O₂) cylinders with a special built gas injection system as shown in Figure 1 (a). For trace quantities of impurity gas, the moles of gas required was obtained by injecting the gas into a cylinder of known volume at known temperature and pressure. The gas was then pushed into the autoclave with CO₂. Gases at higher concentrations were injected directly into the autoclave until the required ΔP was obtained (Figure 1 (b)). The moles of each impurity required to reach the required concentrations was calculated from the Peng-Robinson equation of state.¹⁸ High pressure CO₂ sourced from high-purity bottles was added to the autoclave aided with a gas booster pump to the desired working pressure. An impeller was used to stir the supercritical CO₂ and to generate flow velocities of about 1 m/s (1000 rpm) during the test for the conditions with flow.

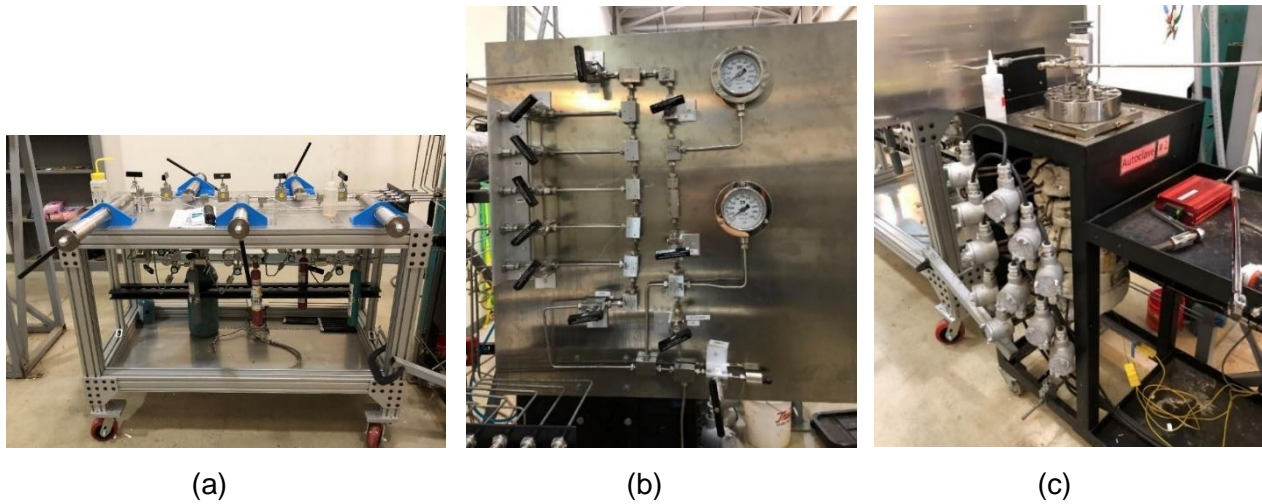


Figure 1: Photographs of the autoclave system used for corrosion testing: (a) impurity injection system, (b) control panel, and (c) autoclave.

The corrosion rates were determined by weight-loss methods at the end of 48 hours exposure. The specimens were removed and cleaned for 5 min in Clarke’s solution (20 g antimony trioxide + 50 g stannous chloride and hydrochloric acid to make 1000 ml). The specimens were then rinsed in distilled water, dried and weighed to 0.1 mg. The corrosion rate can be calculated by the following equation:

$$\text{Corrosion rate (mm/y)} = \frac{8.76 \times 10^4 \times \text{weight loss (g)}}{\text{surface area (cm}^2\text{)} \times \text{density Fe (g/cm}^3\text{)} \times \text{exposure time (hour)}}$$

Following extraction, the morphology and compositions of corrosion products were analyzed by scanning electron microscopy (SEM) and energy dispersive X-ray spectroscopy (EDS). Localized corrosion was measured via surface profilometry after corrosion products were removed. Table 1 shows the detailed test conditions for the present study. The concentrations of impurities are set upon autoclave closure and left to proceed naturally without further additions. Impurity levels were determined based on CO₂ specifications and field conditions provided by the sponsor.¹⁹⁻²¹

Table 1
Test conditions for corrosion testing. Concentrations are initial values set upon autoclave closure.

Test	Material	pCO ₂ (MPa)	Temp. (°C)	H ₂ O (ppm)	SO ₂ (ppm)	NO (ppm)	O ₂ (ppm)	Flow
1	X65	8	35	650	50	100	0	No
2	X65	8	35	650	4500	100	0	No
3	X65	8	35	650	50	100	40,000	No
4	X65	8	35	650	4500	100	40,000	No
5	X65	8	35	650	4500	100	0	Yes
6	X65	8	35	650	4500	100	20,000	Yes
7	X65	8	35	650	4500	100	40,000	Yes
8	X65	8	35	650	50	100	40,000	Yes

RESULTS AND DISCUSSION

Effect of SO₂ and O₂

Figure 2 shows the corrosion rates of carbon steel in the supercritical CO₂ phase with different concentrations of SO₂ and O₂ under quiescent conditions. There was no measurable sample weight change (less than 0.1 mg/cm²) after the test in the presence of 50 ppm of SO₂ with 650 ppm H₂O and 100 ppm NO, indicating an insignificant corrosion rate. However, a moderate corrosion rate was measured (≈ 0.16 mm/y) when the SO₂ concentration increased to 4500 ppm. This corrosion rate is slightly higher than the previous experiments (≈ 0.1 mm/y) conducted under lower SO₂ concentration (1000 ppm).⁷ It is noteworthy that the corrosion rates increased with the addition of 40,000 ppm O₂ for both low (0 to 0.15 mm/y) and high (0.16 to 0.42 mm/y) SO₂ concentrations. This may be due to the formation of sulfuric acid (H₂SO₄) in the presence of O₂.⁶

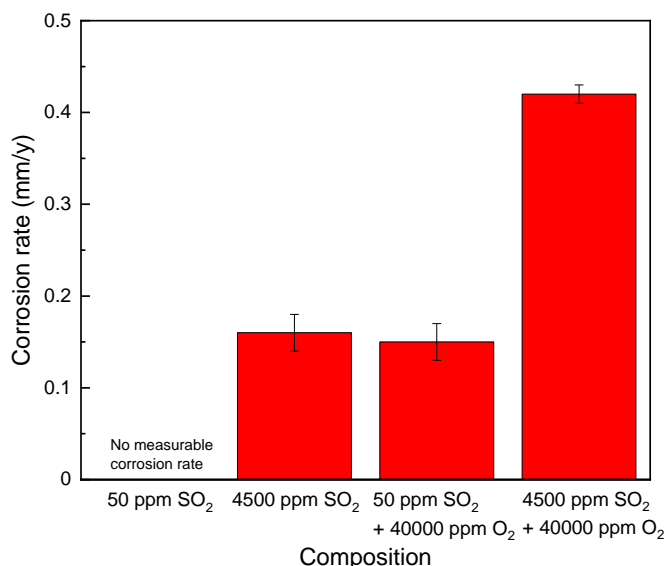


Figure 2: Corrosion rates of X65 carbon steel under supercritical CO₂ with different SO₂ and O₂ concentrations in the absence of flow.

Figure 3 shows pictures of the samples after conducting the corrosion tests in the supercritical CO₂ phase (80 bar and 35°C) with different SO₂ and O₂ concentrations. For the condition with 50 ppm SO₂ (Figure 3 (a)), it can be seen that a majority of the surface was shiny, and no visible signs of corrosion were observed, i.e., the surfaces showed polishing marks. For the condition with 4500 ppm SO₂ (Figure 3 (b)), the formation of scattered corrosion products was observed on the surface of steel. When O₂ was present in the system, the whole surfaces were covered by dark reddish corrosion products (Figure 3 (c), (d)).

Figure 4 shows the SEM image of the surface of the sample after 48 hours exposure in the supercritical CO₂ phase with 650 ppm H₂O, 4500 ppm SO₂, and 100 ppm NO. The surface was covered by corrosion products with cracks, which clearly show the occurrence of corrosion under the testing condition. Table 2 represents EDS analysis of different locations on the sample surface. Location A showed that it was mainly consisted of iron (Fe), oxygen (O) and sulfur (S), suggesting the formation of FeSO₃. Furthermore, areas where no corrosion products were formed were also observed (location B).

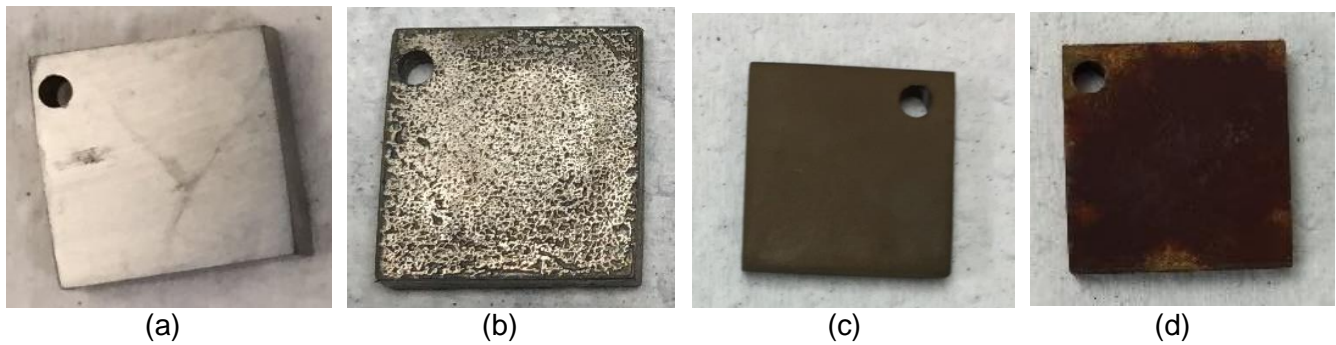


Figure 3: Picture of the surface of the X65 samples after corrosion tests with 650 ppm H₂O and 100 ppm NO at 80 bar and 35°C: (a) Test 1: 50 ppm SO₂, (b) Test 2: 4500 ppm SO₂, (c) Test 3: 50 ppm SO₂ + 40,000 ppm O₂, (d) Test 4: 4500 ppm SO₂ + 40,000 ppm O₂.

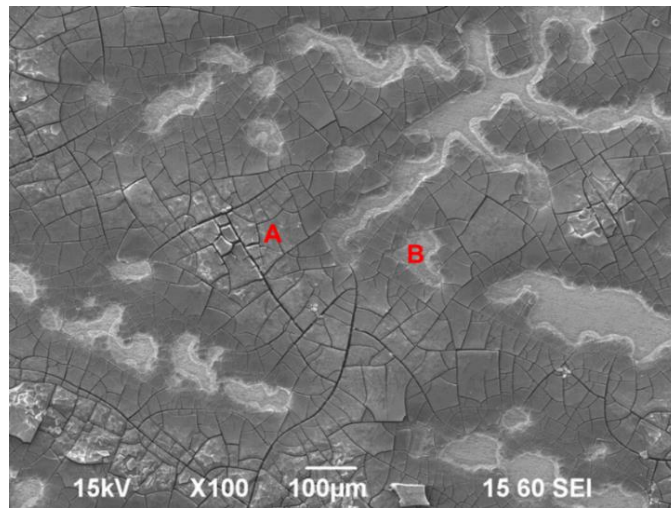


Figure 4: SEM image of the corroded surface of sample exposed to the supercritical CO₂ phase with 650 ppm H₂O, 4500 ppm SO₂ and 100 ppm NO for 48 hours.

Table 2
EDS analysis for different locations of the corroded surface shown in Figure 4.

	Fe (At %)	C (At %)	S (At %)	O (At %)
A	24.05	10.34	29.14	36.47
B	90.56	8.14	1.29	-

Figure 5 shows the SEM image of the surface of the sample after 48 hours exposure in the supercritical CO₂ phase with 650 ppm H₂O, 50 ppm SO₂, 100 ppm NO, and 40000 ppm O₂. The surface was covered by thin corrosion products, which clearly show the occurrence of corrosion under the testing condition. EDS analysis of corrosion products showed that it was mainly consisted of Fe, O and S, indicating the formation of FeSO₄ or Fe₂O₃ (Table 3).

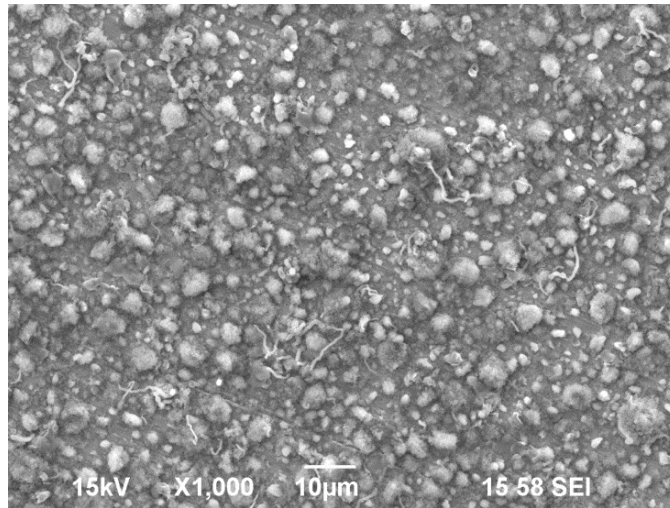


Figure 5: SEM image of the corroded surface of sample exposed to the supercritical CO₂ phase with 650 ppm H₂O, 50 ppm SO₂, 100 ppm NO and 40000 ppm O₂ (Test 3) for 48 hours.

Table 3
EDS analysis of the corroded surface shown in Figure 5.

Fe (At %)	C (At %)	S (At %)	O (At %)
51.06	17.53	2.20	27.59

Figure 6 represents the SEM image of the surface of the sample after 48 hours exposure in the supercritical CO₂ phase with 650 ppm H₂O, 4500 ppm SO₂, 100 ppm NO, and 40,000 ppm O₂. The surface was covered by thick corrosion products. EDS analysis of corrosion products showed that although the morphology of the corrosion product is different, the constituent elements are the same (Fe, O and S), indicating the formation of FeSO₄ or Fe₂O₃ (Table 4).

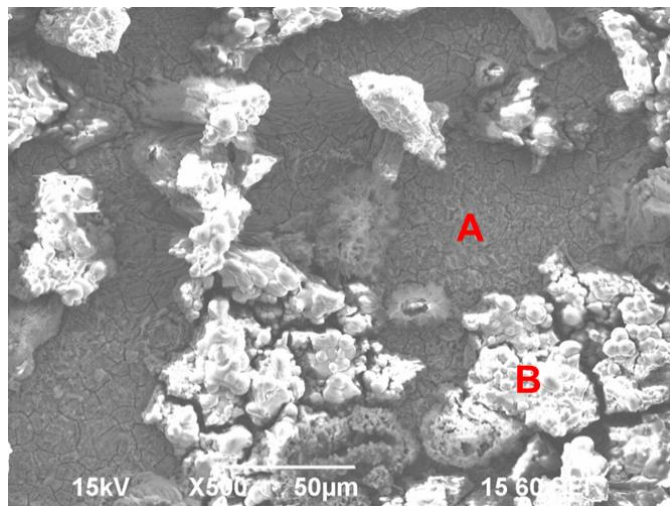


Figure 6: SEM image spectra of the corroded surfaces of sample exposed to the supercritical CO₂ phase with 650 ppm H₂O, 4500 ppm SO₂, 100 ppm NO and 40000 ppm O₂ (Test 4) for 48 hours.

Table 4
EDS analyses of the corroded surface shown in Figure 6.

At.%	Fe	C	S	O
A	57.82	4.69	2.74	33.11
B	19.31	15.42	2.36	60.49

Figure 7 represents the surface morphologies of samples after removing the corrosion products. No localized corrosion was observed on the surface (uniform corrosion) for all three different conditions.

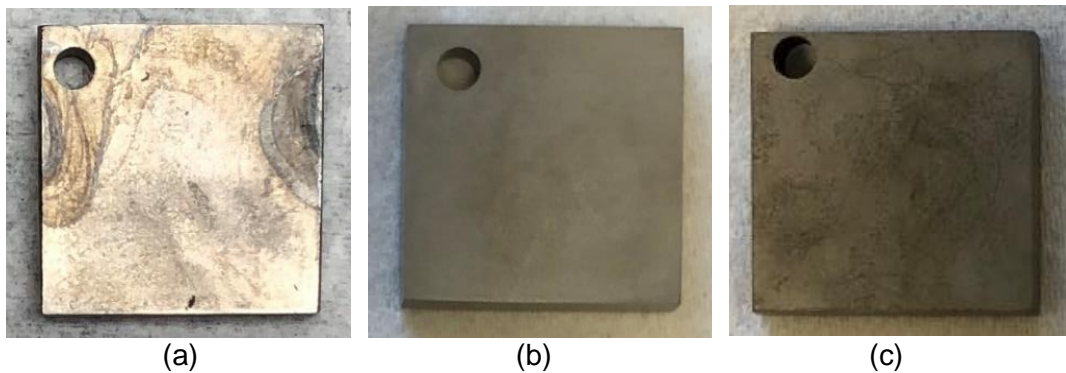


Figure 7: Picture of the surface of the samples after cleaning: (a) Test 2: 4500 ppm SO₂, (b) Test 3: 50 ppm SO₂ + 40,000 ppm O₂, (c) Test 4: 4500 ppm SO₂ + 40,000 ppm O₂.

Effect of Flow

Figure 8 shows the corrosion rates of carbon steel in the flowing supercritical CO₂ phase (650 ppm H₂O, 4500 ppm SO₂ and 100 ppm NO) with different O₂ concentrations. Comparing with the corrosion rate without flow, the presence of flow increased the corrosion rate from 0.16 mm/y to 1.30 mm/y. Although the addition of 20,000 ppm O₂ doesn't affect the general corrosion rate under flowing condition, the corrosion rate significantly increased when 40,000 ppm O₂ was added.

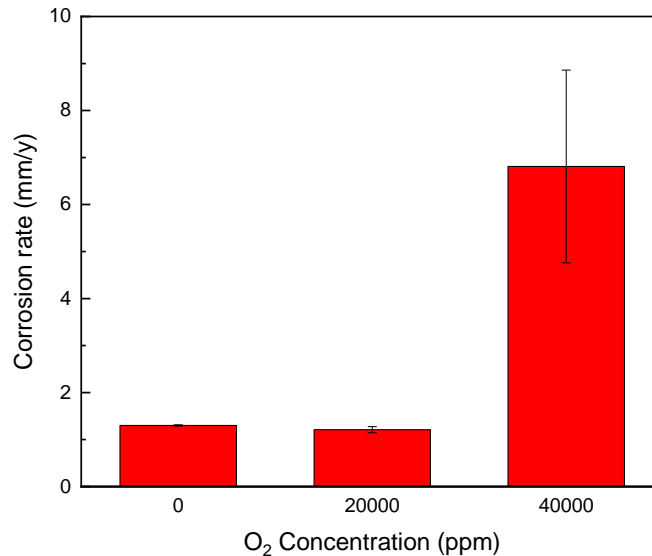


Figure 8: Corrosion rates of carbon steel under flowing supercritical CO₂ with different O₂ concentrations (650 ppm H₂O, 4500 ppm SO₂, and 100 ppm NO).

Figure 9 shows pictures of the samples after conducting the corrosion tests in the flowing supercritical CO₂ phase with different O₂ concentrations. In the absence of O₂, a blackish corrosion product was formed, whereas a redish corrosion product was observed in the presence of O₂.

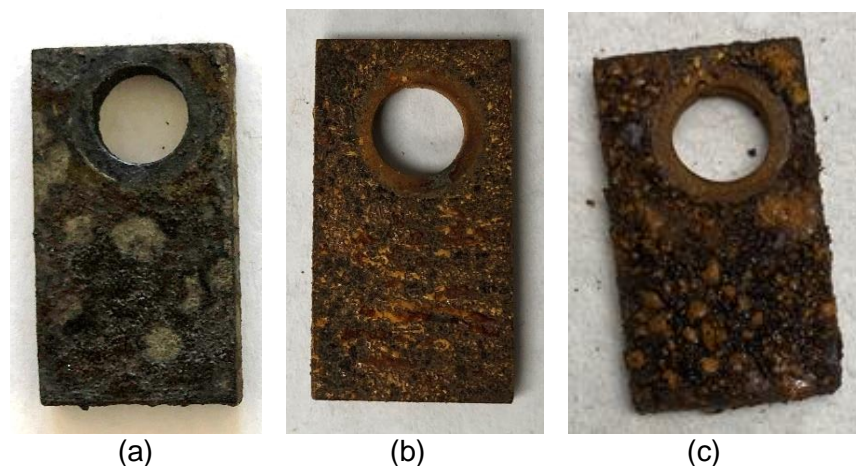


Figure 9: Pictures of the surface of the samples after corrosion tests with 650 ppm H₂O, 4500 ppm SO₂ and 100 ppm NO at 80 bar CO₂ and 35°C with 1000 rpm of flow: (a) Test 5: 0 ppm O₂, (b) Test 6: 20,000 ppm O₂, (c) Test 7: 40,000 ppm O₂.

Figure 10 shows the SEM image of the surface of the sample from Test 5 after 48 hours exposure in the flowing supercritical CO₂ phase with 650 ppm H₂O, 4500 ppm SO₂, and 100 ppm NO. The surface was covered with a dense crystalline corrosion products. EDS analyses of corrosion products showed that the corrosion products were mainly consisted of Fe, S and O (Table 5), indicating the formation of FeSO₃.

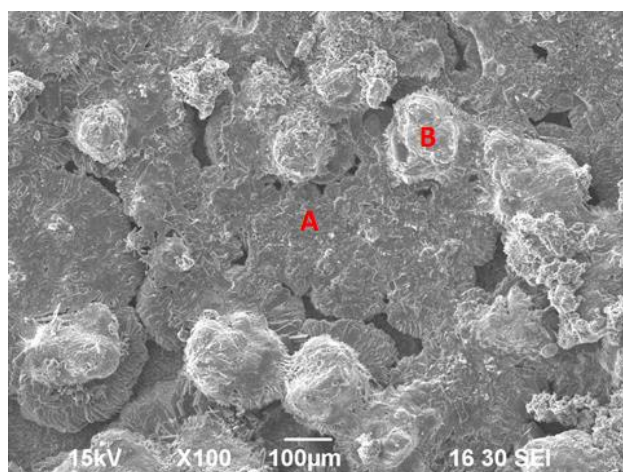


Figure 10: SEM image of the corroded surface of sample exposed to the flowing supercritical CO₂ phase with 650 ppm H₂O, 4500 ppm SO₂ and 100 ppm NO for 48 hours (Test 5).

Table 5
EDS analysis for different locations of the corroded surface in Figure 10.

At.%	Fe	C	S	O
A	23.24	10.69	26.38	39.70
B	14.34	13.60	22.91	49.15

Figure 11 represents the results of high-resolution optical profilometry analysis of several pits observed on the cleaned samples exposed to the flowing supercritical CO₂ phase with 650 ppm H₂O, 4500 ppm

SO₂, 100 ppm NO, and 20,000 ppm O₂ for 48 hours. Although the presence of flow increased general corrosion rate, no localized corrosion was observed on the surface (uniform corrosion) in the absence of O₂.

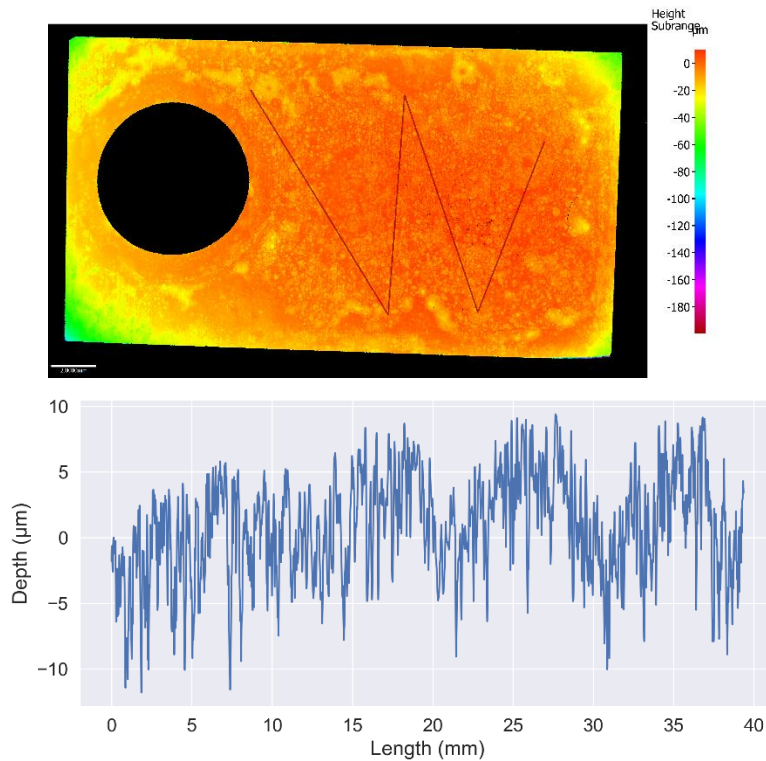


Figure 11: Optical profilometry analysis of the sample surface exposed to the flowing supercritical CO₂ phase with 650 ppm H₂O, 4500 ppm SO₂, and 100 ppm NO for 48 hours.

Figure 12 shows the SEM image of the surface of the sample from Test 6 after 48 hours exposure in the flowing supercritical CO₂ phase with 650 ppm H₂O, 4500 ppm SO₂, 100 ppm NO, and 20,000 ppm O₂. The surface was covered with non-uniform corrosion products. EDS analyses of corrosion products showed that both inner (location A and B) and outer (location C) corrosion products were mainly consisted of Fe, C, S and O, but outer corrosion product has more S (Table 6).

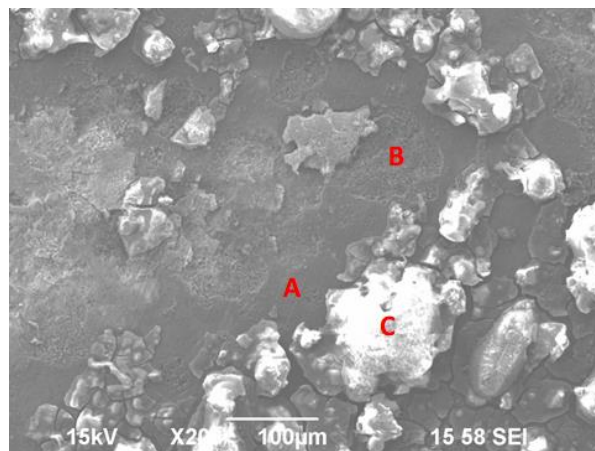


Figure 12: SEM image of the corroded surface of sample exposed to the flowing supercritical CO₂ phase with 650 ppm H₂O, 4500 ppm SO₂, 100 ppm NO and 20,000 ppm O₂ (Test 6) for 48 hours.

Table 6
EDS analysis for different locations of the corroded surface in Figure 12.

At.%	Fe	C	S	O
A	38.36	20.49	0.28	40.87
B	42.63	22.48	0.39	34.49
C	41.45	13.16	5.02	40.37

Figure 13 presents the results of high-resolution optical profilometry analysis of several pits observed on the cleaned samples exposed to the flowing supercritical CO₂ phase with 650 ppm H₂O, 4500 ppm SO₂, 100 ppm NO, and 20,000 ppm O₂ for 48 hours. According to the depth of the deepest pit (92.8 μm), the maximum localized corrosion rate was calculated to be 16.9 mm/y, which is almost 13 times higher than the general corrosion rate, indicating that the presence of O₂ and flow caused a localized corrosion under this condition.

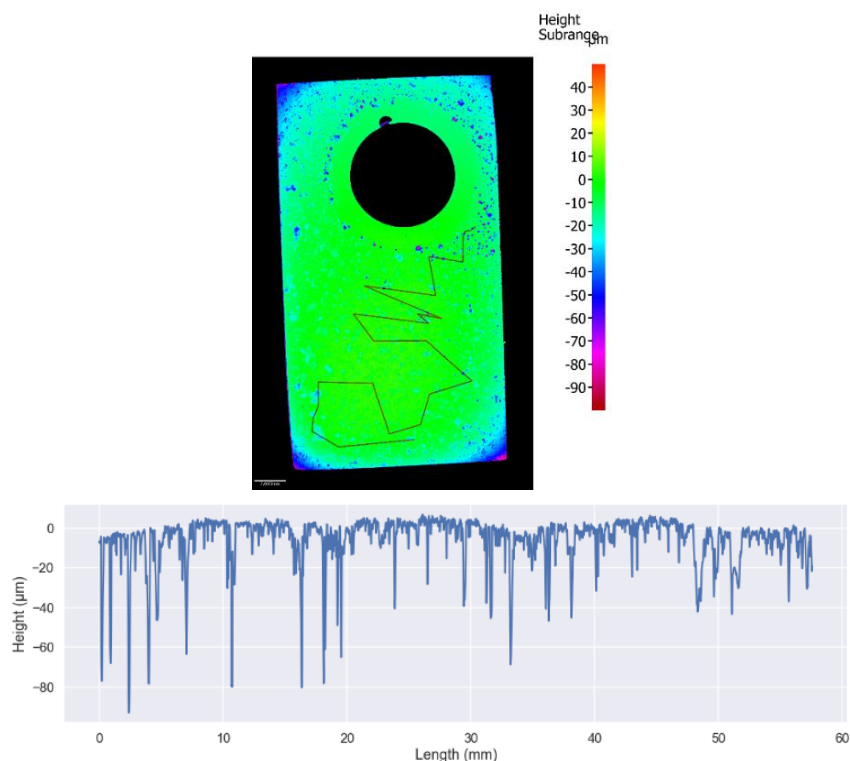


Figure 13: Optical profilometry analysis of the sample surface exposed to the flowing supercritical CO₂ phase with 650 ppm H₂O, 4500 ppm SO₂, 100 ppm NO and 20,000 ppm O₂ (Test 6) for 48 hours.

Figure 14 shows the SEM image of the surface of the sample from Test 7 after 48 hours exposure in the flowing supercritical CO₂ phase with 650 ppm H₂O, 4500 ppm SO₂, 100 ppm NO, and 40,000 ppm O₂. Similar to the condition with 20,000 ppm O₂, the surface was covered with non-uniform corrosion products. EDS analyses of corrosion products showed that inner (location A) corrosion products were mainly consisted of Fe, C, S and O, whereas the outer (location B) corrosion products were mainly consisted of Fe, C and O (Table 7).

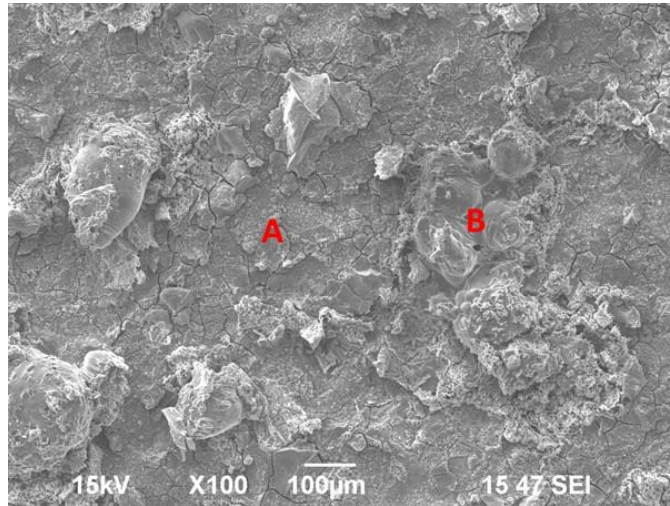
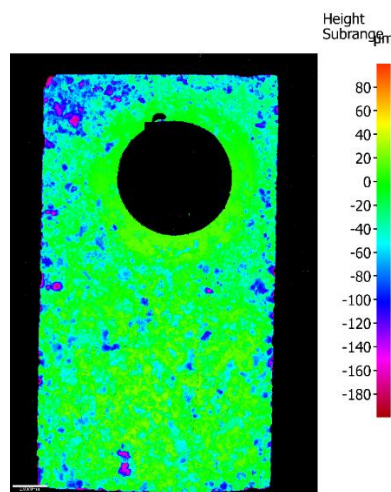


Figure 14: SEM image of the corroded surface of sample exposed to the flowing supercritical CO₂ phase with 650 ppm H₂O, 4500 ppm SO₂, 100 ppm NO and 40000 ppm O₂ (Test 7) for 48 hours.

Table 7
EDS analysis for different locations of the corroded surface in Figure 14.

At.%	Fe	C	S	O
A	58.21	10.55	1.72	29.52
B	46.72	3.56	-	49.72

Figure 15 presents the results of high-resolution optical profilometry analysis of several pits observed on the cleaned samples exposed to the flowing supercritical CO₂ phase with 650 ppm H₂O, 4500 ppm SO₂, 100 ppm NO, and 40,000 ppm O₂ for 48 hours. According to the depth of the deepest pit (170.5 µm), the maximum localized corrosion rate was calculated to be 31.1 mm/y, which is almost 4 times higher than the general corrosion rate, indicating again that the presence of O₂ and flow caused a localized corrosion.



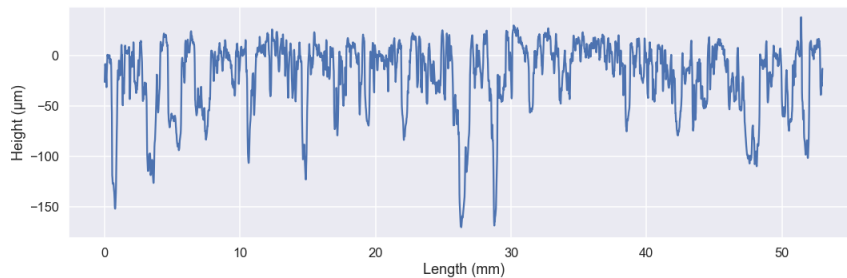


Figure 15: Optical profilometry analysis of the sample surface exposed to the flowing supercritical CO₂ phase with 650 ppm H₂O, 4500 ppm SO₂, 100 ppm NO and 40000 ppm O₂ for 48 hours.

Figure 16 shows pictures of the sample after conducting the corrosion Test 8 in the flowing supercritical CO₂ phase (80 bar and 35°C) with 650 ppm H₂O, 50 ppm SO₂, 100 ppm NO and 40,000 ppm O₂. It can be clearly seen that the presence of flow accelerated the corrosion even with low concentration of SO₂. Figure 17 shows the SEM image of the surface of the sample after 48 hours exposure. The surface was covered with a dense inner corrosion product and a loose outer corrosion product. EDS analyses of corrosion products showed that both inner and outer corrosion products were mainly consisted of Fe, S and O, but outer corrosion product has more S and O (Table 8).



Figure 16: Pictures of the surface of the samples after corrosion Test 8 with 650 ppm H₂O, 50 ppm SO₂, 100 ppm NO and 4% O₂ at 80 bar CO₂ and 35°C with 1000 rpm of flow.

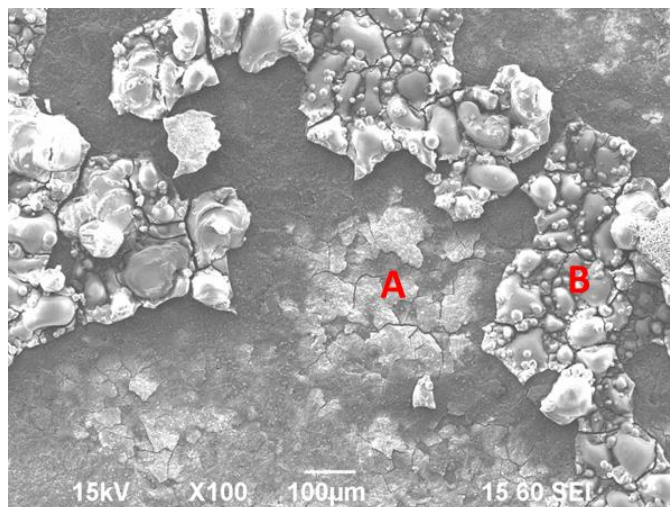
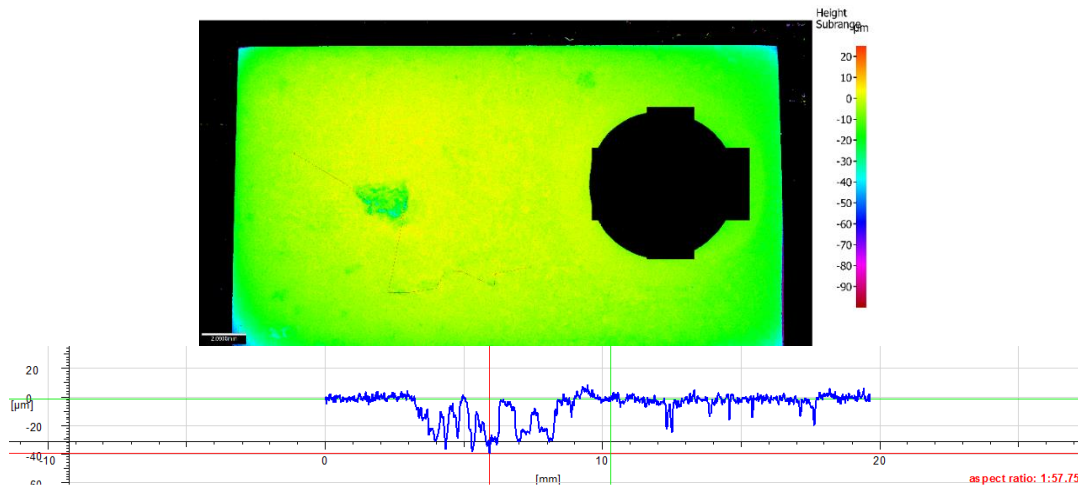


Figure 17: SEM image of the corroded surface of sample exposed to the flowing supercritical CO₂ phase with 650 ppm H₂O, 50 ppm SO₂, 100 ppm NO and 4% O₂ (Test 8) for 48 hours.

Table 8: EDS analysis for different locations of the corroded surface shown in Figure 17.

At.%	Fe	C	S	O
A	46.89	9.76	1.97	41.39
B	19.97	10.34	9.10	60.59

Figure 18 presents the result of high-resolution optical profilometry analysis of several pits observed on the cleaned samples exposed to the flowing supercritical CO₂ phase with 650 ppm H₂O, 50 ppm SO₂, 100 ppm NO and 40,000 ppm O₂ for 48 hours. According to the depth of the deepest pit (39.8 μm), the maximum localized corrosion rate was measured to be 7.27 mm/y.



(b)

Figure 18: Optical profilometry analysis of the sample surface exposed to the flowing supercritical CO₂ phase with 650 ppm H₂O, 50 ppm SO₂, 100 ppm NO and 4% O₂ (Test 8) for 48 hours.

Figure 19 compares the uniform and localized corrosion rates of carbon steel in the flowing supercritical CO₂ phase with different SO₂ concentrations in the presence of 40,000 ppm O₂. When both flow and O₂ are present, localized corrosion occurs regardless of the concentration of SO₂, whereas the uniform corrosion and localized corrosion rates increase as the concentration of SO₂ increases.

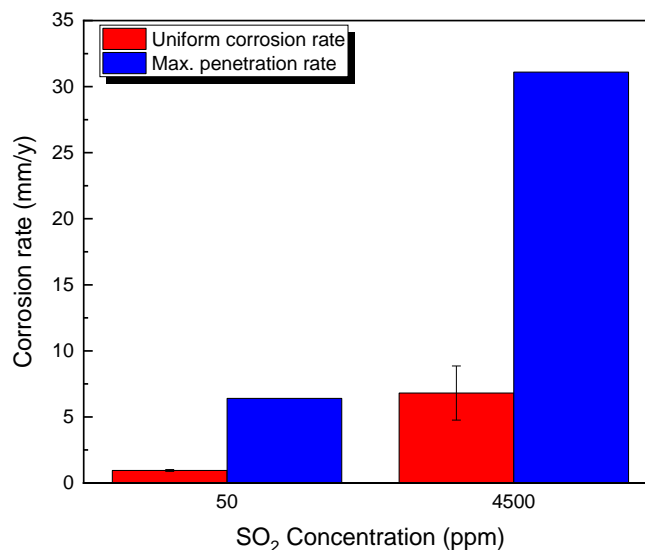


Figure 19: Comparison of uniform and localized corrosion rates under flowing supercritical CO₂ with different SO₂ concentrations (650 ppm H₂O, 100 ppm NO, and 40,000 ppm O₂).

It is hypothesized that a primary cause of accelerated corrosion due to flow is that the flow increased the chance of condensed acids reaching the surface of the steel specimens. The flowing supercritical CO₂ could potentially aid condensed acids droplets reaching the steel surface thereby replenishing the acid species required for corrosion. This mechanism was likewise attributed to accelerated corrosion by Liu, et al.¹⁵ The mechanism of localized corrosion is far less certain. Further work is required to examine the relationship of the impurities and flow with localized corrosion.

CONCLUSIONS

Table 9 shows the summary of the autoclave corrosion tests. In the supercritical CO₂ phase (8 MPa, 35°C) with 650 ppm H₂O and 100 ppm NO, the corrosion rates depended on the SO₂ and O₂ concentrations, and the presence of flow. The corrosion rates increased from 0 to 0.16 mm/y with increasing SO₂ content from 50 ppm to 4500 ppm in the stagnant condition. With low SO₂ content (50 ppm), addition of 40,000 ppm O₂ slightly affect the corrosion rate, however, the corrosion rate increased from 0.16 to 0.42 mm/y in the presence of 4500 ppm SO₂ and 40,000 O₂ under stagnant condition. The presence of flow significantly accelerated the corrosion of carbon steel hypothesized to be due to the addition of acids condensed elsewhere than the steel specimen. The corrosion rate increased from 0.16 mm/y to 1.30 mm/y with 4500 ppm SO₂. Furthermore, significant localized corrosion was observed in the presence of both O₂ and flow. 6.4 mm/y of the maximum penetration rate was measured for the condition with 50 ppm SO₂ and 40,000 ppm O₂. And much higher penetration rate (31.1 mm/y) was measured for the condition with 4500 ppm SO₂ and 40,000 ppm O₂.

Table 9: Summary of the autoclave corrosion tests.

Test	pCO ₂ (bar)	Temp. (°C)	H ₂ O (ppm)	SO ₂ (ppm)	NO (ppm)	O ₂ (ppm)	Flow	Corrosion Rate (mm/y)	Localized Corrosion
1	80	35	650	50	100	0	No	0	No
2	80	35	650	4500	100	0	No	0.16	No
3	80	35	650	50	100	40,000	No	0.15	No
4	80	35	650	4500	100	40,000	No	0.42	No
5	80	35	650	4500	100	0	Yes	1.30	No
6	80	35	650	4500	100	20,000	Yes	1.21	Yes (13.1 mm/y)
7	80	35	650	4500	100	40,000	Yes	6.81	Yes (31.1 mm/y)
8	80	35	650	50	100	40,000	Yes	0.95	Yes (6.4 mm/y)

ACKNOWLEDGEMENTS

The authors would like to acknowledge the financial support from Ohio Coal Development Office (OCDO) for the Institute for Corrosion and Multiphase Technology at Ohio University.

REFERENCES

1. Y.C. Zhang, K.W. Gao, G. Schmitt, "Water Effect On Steel Under Supercritical CO₂ Condition," CORROSION/2011, paper no. 11378 (Houston, TX: NACE, 2011).
2. Y. Xiang, Z. Wang, X. X. Yang, Z. Li, W. D. Ni, "The Upper Limit of Moisture Content for Supercritical CO₂ Pipeline Transport," *Journal of Supercritical Fluid* 67 (2012): p. 14.
3. Y. Hua, R. Barker, A. Neville, "Effect of Temperature on the Critical Water Content for General and Localised Corrosion of X65 Carbon Steel in the Transport of Supercritical CO₂," *International Journal of Greenhouse Gas Control* 31 (2014): p. 48.

4. Y. Hua, R. Barker, A. Neville, "Comparison of Corrosion Behaviour for X-65 Carbon Steel in Supercritical CO₂-Saturated Water and Water-Saturated/Unsaturated Supercritical CO₂," *Journal of Supercritical Fluid* 97 (2015): p. 224.
5. X. Jiang, D. Qu, X. Song, X. Liu, Y. Zhang, "Critical water content for corrosion of X65 mild steel in gaseous, liquid and supercritical CO₂ stream," *International Journal of Greenhouse Gas Control* 85 (2019): p. 11.
6. Y.S. Choi, S. Nestic, D. Young, "Effect of Impurities on the Corrosion Behavior of CO₂ Transmission Pipeline Steel in Supercritical CO₂-Water Environments," *Environ. Sci. Technol.* 44 (2010): p. 9233.
7. F. Farelas, Y.S. Choi, S. Nestic, "Corrosion Behavior of API 5L X65 Carbon Steel Under Supercritical and Liquid Carbon Dioxide Phases in the Presence of Water and Sulfur Dioxide," *Corrosion* 69 (2013): p. 243.
8. Y. Hua, R. Barker, A. Neville, "The Effect of O₂ Content on the Corrosion Behaviour of X65 and 5Cr in Water-Containing Supercritical CO₂ Environments," *Applied Surface Science* 356 (2015): p. 499.
9. Y. Hua, R. Barker, A. Neville, "The Influence of SO₂ on the Tolerable Water Content to Avoid Pipeline Corrosion during the Transportation of Supercritical CO₂," *International Journal of Greenhouse Gas Control* 37 (2015): p. 412.
10. M. Xu, Q. Zhang, X. X. Yang, Z. Wang, J. Liu, Z. Li, "An Experimental Investigation of Supercritical CO₂ Accidental release from a Pressurized Pipeline," *Journal of Supercritical Fluid* 107 (2016): p. 286.
11. A. Dugstad, M. Halseid, "Internal Corrosion In Dense Phase CO₂ Transport Pipelines - State of the Art And the Need For Further R&D," CORROSION 2012, paper no. 0001452 (Houston, TX: NACE, 2011).
12. Y.S. Choi, S. Hassani, T. N. Vu, S. Nestic, A.Z.B. Abas, "Effect of H₂S on the Corrosion Behavior of Pipeline Steels in Supercritical and Liquid CO₂ Environments," *Corrosion* 72 (2016): p. 999.
13. G. Cui, Z. Yang, J. Liu, Z. Li, "A Comprehensive Review of Metal Corrosion in a Supercritical CO₂ Environment," *International Journal of Greenhouse Gas Control* 90 (2019): p. 102814.
14. W. Wang, K. Shen, S. Tang, R. Shen, T. Parker, Q. Wang, "Synergistic Effect of O₂ and SO₂ Gas Impurities on X70 Steel Corrosion in Water-Saturated Supercritical CO₂," *Process Safety and Environmental Protection* 130 (2019): p. 57.
15. A.Q. Liu, C. Bian, Z.M. Wang, X. Han, J. Zhang, "Flow dependence of steel corrosion in supercritical CO₂ environments with different water concentrations," *Corrosion Science* 134 (2018) 149-161.
16. P. Sui, J. Sun, C. Sun, Y. Wang, Y. Hua, "The Influence of Flow Rate on Corrosion Behavior of X65 Carbon Steel in Water-saturated Supercritical CO₂/H₂S System," CORROSION 2019, paper no. 13081 (Houston, TX: NACE, 2019).
17. Y.S. Choi, S. Nestic, "Determining the corrosive potential of CO₂ transport pipeline in high pCO₂-water environments," *International Journal of Greenhouse Gas Control* 5 (2011): p. 788.
18. D.Y. Peng, D.B. Robinson, "A New Two-Constant Equation of State," *Industrial & Engineering Chemistry Fundamentals* 15 (1976): p. 59
19. A. Dugstad, M. Halseid, B. Morland, "Testing of CO₂ Specifications With Respect to Corrosion and Bulk Phase Reactions," *Energy Procedia* 63 (2014): p. 2547.
20. DOE/NETL Quality Guidelines for Energy System Studies, "CO₂ impurity design Parameters", DOE/NETL-341/011212, 2013.
21. A. Armpriester, "W.A. Parish Post Combustion CO₂ Capture and Sequestration Project Final Public Design Report". United States. doi.: <https://www.osti.gov/servlets/purl/1344080>, 2017.